

# GlimmerNet: A Lightweight Grouped Dilated Depthwise Convolutions for UAV-Based Emergency Monitoring

Dorđe Nedeljković  
Independent Researcher  
djordjened92@gmail.com

## Abstract

*Convolutional Neural Networks (CNNs) have proven highly effective for edge and mobile vision tasks due to their computational efficiency. While many recent works seek to enhance CNNs with global contextual understanding via self-attention-based Vision Transformers, these approaches often introduce significant computational overhead. In this work, we demonstrate that it is possible to retain strong global perception without relying on computationally expensive components.*

*We present GlimmerNet, an ultra-lightweight convolutional network built on the principle of separating receptive field diversity from feature recombination. GlimmerNet introduces Grouped Dilated Depthwise Convolutions (GDBlocks), which partition channels into groups with distinct dilation rates, enabling multi-scale feature extraction at no additional parameter cost. To fuse these features efficiently, we design a novel Aggregator module that recombines cross-group representations using grouped pointwise convolution, significantly lowering parameter overhead. With just **31K** parameters and **29% fewer FLOPs** than the most recent baseline, GlimmerNet achieves a new state-of-the-art weighted **F1-score of 0.966** on the UAV-focused AIDERv2 dataset. These results establish a new accuracy–efficiency trade-off frontier for real-time emergency monitoring on resource-constrained UAV platforms. Our implementation is publicly available at <https://github.com/djordjened92/gdd-cnn>.*

## 1. Introduction

Unmanned aerial vehicles (UAVs) are a common tool for image collection across various applications. One particularly practical domain is emergency response, where aerial views provide a secure and efficient way to plan rescue operations. UAVs are typically affordable and effective for monitoring hard-to-reach areas. However, they often come with limited onboard computational resources.

This constraint has led to active research in developing efficient computer vision methods suitable for such environments. Specifically, battery-powered embedded systems push researchers to adapt dominant architectures like CNNs and Transformers [30] to operate with fewer parameters while retaining high performance. A key challenge in this field is identifying the minimum model size and computational load needed for specific tasks.

To address this, we introduce GlimmerNet, an extremely lightweight CNN-based architecture. After an initial Stem block that downsamples the input resolution, GlimmerNet employs four stages of depthwise convolutional blocks. Each stage has multiple blocks with **grouped depthwise convolutions**, where every group has a **distinct dilation rate**. This approach is drawing an inspiration from Mix-Conv [28], which varies kernel sizes across groups. This design allows the network to capture multiple receptive field sizes within a single convolutional layer.

Our main architectural innovation lies in how we **aggregate** the outputs from these convolutional groups. Instead of the conventional  $1 \times 1$  full dense convolution (which is parameter-heavy), we propose a novel *Aggregator* block. This block reorganizes the feature maps into new groups and applies a  $1 \times 1$  grouped convolution, reducing the parameter count significantly.

Compared to the recent lightweight model TakuNet [20], which also uses depthwise convolutions, our **grouped dilated depthwise convolutions** and **aggregation strategy** allows reduced number of convolutional blocks and smaller network size while achieving better accuracy.

The primary performance evaluation of GlimmerNet is conducted using the publicly available AIDERv2 [23] dataset, which includes images of various emergency scenarios such as earthquakes, floods, and fires.

Our contributions go beyond conventional lightweight CNNs by decoupling receptive-field expansion from channel mixing, allowing GlimmerNet to scale multi-dilation context without increasing computational cost.

**1. A new architectural principle for resource-bounded UAV perception.** Unlike MobileNet [7], MixNet-S [28],

and TakuNet [20] which expand receptive fields mainly by depth or width increase, we introduce a dual-path design that separates receptive field diversity from feature recombination. This enables multi-scale perception within a single block, making GlimmerNet particularly suitable for on-board UAV inference where FLOPs and memory are constrained.

2. **Grouped Dilated Depthwise Convolutions (GDBlocks) for multi-scale context at constant cost.** We propose a convolutional unit that assigns distinct dilation rates to grouped depthwise kernels, producing  $m$  simultaneous receptive field scales without additional parameters or MACs. In contrast to previous dilation-based models, GDBlocks achieve multi-scale coverage inside one operation.
3. **Efficient Aggregator for feature fusion.** We propose a lightweight Aggregator module that reorganizes and fuses multi-scale features using grouped pointwise convolutions, achieving low-cost cross-group interaction compared to dense fusion in prior works.
4. **Improved accuracy–efficiency trade-off.** Through the synergy of GDBlocks and the Aggregator, GlimmerNet achieves **16.6%** fewer parameters and **29%** fewer FLOPs than TakuNet [20], while delivering superior classification accuracy on AIDERv2 [23].

This demonstrates that **receptive field diversity and lightweight feature fusion can outperform conventional block stacking**, advancing the design of compact CNNs for embedded intelligence.

## 2. Related work

Many on-device computer vision applications require models that keep a balance between computational efficiency and high classification accuracy. This need has led to the development of two complementary streams of research: general-purpose lightweight architectures and domain-specific neural network designs.

### 2.1. Efficient Architectures

SqueezeNet [9] is one of the earliest CNN architectures explicitly designed for efficiency. It achieves parameter reduction by replacing most standard convolutions with  $1 \times 1$  convolutions for dimensionality reduction, followed by  $3 \times 3$  convolutions for spatial feature learning. A widely adopted family in the mobile-scale model domain is MobileNet [7], with V2 [21] and V3 [8] variants. These models introduce and refine the use of depthwise separable convolutions, where spatial filtering is performed by depthwise convolutions and feature aggregation across channels is handled by pointwise convolutions. Later versions improve this design with inverted residual blocks and optimized architecture search strategies. A similar idea is in the core of ShuffleNetV1 [34] and ShuffleNetV2 [16],

which enhance efficiency via grouped pointwise convolutions and introduce channel shuffling to enable information flow across groups. EfficientNet [27] applies a compound scaling strategy, jointly optimizing network depth, width, and resolution-guided by Neural Architecture Search (NAS). More recently, ConvNeXt [15] has emerged as a competitive fully convolutional alternative to Vision Transformers. It blends several architectural innovations, including multi-branch grouping strategies inspired by ResNeXt, patchified inputs like in Vision Transformers, and large kernel convolutions in later stages to enhance receptive field and contextual modeling.

Vision Transformers (ViTs) [1] introduced a Transformer-based paradigm to the field of computer vision, initially popularized by the seminal ViT model. While early small ViT variants demonstrated strong performance, they were often challenged by high computational costs and limited optimization for resource-constrained environments. To address these issues, the MobileViT [17, 18] family of models proposed a more efficient hybrid architecture that combines the strengths of convolutional networks for capturing local spatial patterns and Transformer encoders for modeling global dependencies. In MobileViT [17], standard  $n \times n$  convolutions are used for spatial representation learning, followed by pointwise convolutions for projecting features into a higher-dimensional space before applying the Transformer blocks. Unlike traditional ViTs that flatten image patches into 2D sequences, MobileViT [17] preserves both the spatial arrangement of patches and the internal pixel structure within each patch, thereby retaining spatial inductive bias. This architectural choice allows MobileViT [17] to integrate the efficiency of MobileNetV2 [21] blocks with the expressiveness of self-attention, achieving competitive performance with significantly lower computational overhead.

### 2.2. Emergency Response Related Work

An early architecture addressing aerial image recognition in emergency scenarios with the capability to operate on UAV-scale hardware is EmergencyNet [14]. The authors employed multiple dilation rates on the same input tensor to facilitate multi-resolution feature extraction. In contrast to our approach, EmergencyNet [14] applies separate convolutions to the **entire input** for each dilation rate, followed by a **full dense** pointwise convolution to fuse cross-channel information. They also explore various strategies for merging the outputs of the multi-dilated convolutions, such as concatenation, summation, and mean pooling, prior to the fusion step. TinyEmergencyNet [19] builds upon this by introducing channel-wise pruning, effectively reducing model size by up to 50%, making it even more suitable for deployment on constrained hardware.

DiRecNet [23] is a fully convolutional architecture de-

signed specifically for disaster recognition. It incorporates larger kernels (specifically  $7 \times 7$  and  $5 \times 5$ ) early in the network to capture broad contextual features, aligning with the recent trend toward large-kernel CNNs. Later layers utilize depthwise separable  $3 \times 3$  convolutions for increased efficiency.

Its successor, DiRecNetV2 [22], enhances the architecture by using DiRecNet [23] as a feature extractor, followed by two standard Vision Transformer (ViT) [1] encoder blocks. These Transformer layers operate on the latent feature maps of spatial resolution  $14 \times 14$  and channel depth of 192, thereby combining the strengths of CNN-based spatial encoding with Transformer-based global reasoning.

Models like DiRecNetV2 [22] maximize accuracy but are too large, while models like TinyEmergencyNet [19] or TakuNet [20] are efficient but still constrained by redundant or uniform processing.

### 2.3. Comparison With Existing Lightweight Architectures

Lightweight CNNs for aerial perception typically fall into two design patterns:

- improving efficiency through depthwise separable convolutions and
- enlarging receptive fields using dilated or multi-branch kernels.

MobileNetV2 [21], MobileNetV3 [6], ShuffleNetV2 [16], MixNet [28] and EfficientNet [27] are examples of the first category, achieving low computational cost through inverted bottlenecks and pointwise channel expansion. However, these networks predominantly operate with a fixed receptive-field scale per layer, requiring increased depth or multi-branch structures to capture long-range context, what is costly for on-board UAV hardware.

Dilation-based architectures tackle this limitation by enlarging receptive fields without increasing parameters, as in MixNet [28], WaveMix [11], and EmergencyNet [14], but they typically apply one dilation rate per layer, requiring multiple stacked blocks to capture diverse scales.

In contrast, GlimmerNet departs from both families. Our *GDBlock* applies multiple dilation rates simultaneously within a single depthwise operation, producing diverse receptive fields without adding parameters or MACs. Furthermore, the proposed *Aggregator* performs cross-scale recombination using grouped  $1 \times 1$  projections, reducing channel-mixing cost by a factor of  $1/m$  while improving feature diversity.

While prior models excel either in efficiency or contextual perception (dilated models, Transformer hybrids), GlimmerNet integrates both properties within a unified module, capturing multi-scale structure at depthwise cost and fusing it efficiently through grouped projection. The

resulting architecture achieves a more favorable accuracy–efficiency balance compared to existing lightweight CNNs, validated experimentally in 4.

## 3. Methodology

The overall architecture of GlimmerNet, shown in Fig. 1, consists of an initial *Stem* [20] block for input downsampling, followed by four sequential *Stage* blocks. These are succeeded by a *Refiner* [20] block, and finally a classification *Head* [20] that produces the output predictions.

### 3.1. Stem

The *Stem* [20] block is adapted from prior efficient architectures for emergency response, such as TakuNet [20] and EmergencyNet [14]. Its primary function is to significantly reduce the input resolution at an early stage, contributing to overall computational efficiency.

The block begins with a dense convolution, which, although relatively expensive in terms of parameter count, is retained due to its high representational capacity and full inter-channel connectivity. This is the only dense convolution used in the entire GlimmerNet architecture. It is followed by a lightweight depthwise convolution, which maintains spatial processing with minimal additional parameters.

Each convolutional layer in the *Stem* [20] block is followed by standard operations, including Batch Normalization [10] and ReLU6 activation, to ensure stable training and non-linearity.

### 3.2. Stage

The *Stage* serves as the central architectural unit in our design. Following the TakuNet [20] model, we employ four successive *Stages*, each reducing the spatial dimensions while increasing the number of output channels.

In TakuNet [20], a *Stage* consists of several sequential Taku Blocks [20], which are depthwise convolutions combined with Batch Normalization [10] and ReLU6 activation, enhanced by identity skip connections. The output of the Taku Blocks [20] is concatenated with the *Stage*’s input and passed through a pointwise ( $1 \times 1$ ) grouped convolution with fixed group size of 4, followed by spatial downsampling via simple pooling operators.

We adopt this overall structure but introduce key modifications. Specifically, we replace the Taku Blocks [20] with a *GDBlocks*, which utilizes grouped dilated depthwise convolutions. All *GDBlocks* of the single *Stage* are uniformly structured. Additionally, we introduce a novel dedicated Aggregator block that processes the concatenated output of the *GDBlocks* along with the original input to the *Stage*.

Thanks to the efficiency of this **GDBlocks-Aggregator combination**, we require fewer *GDBlocks* per *Stage* compared to the number of Taku Blocks [20] used in

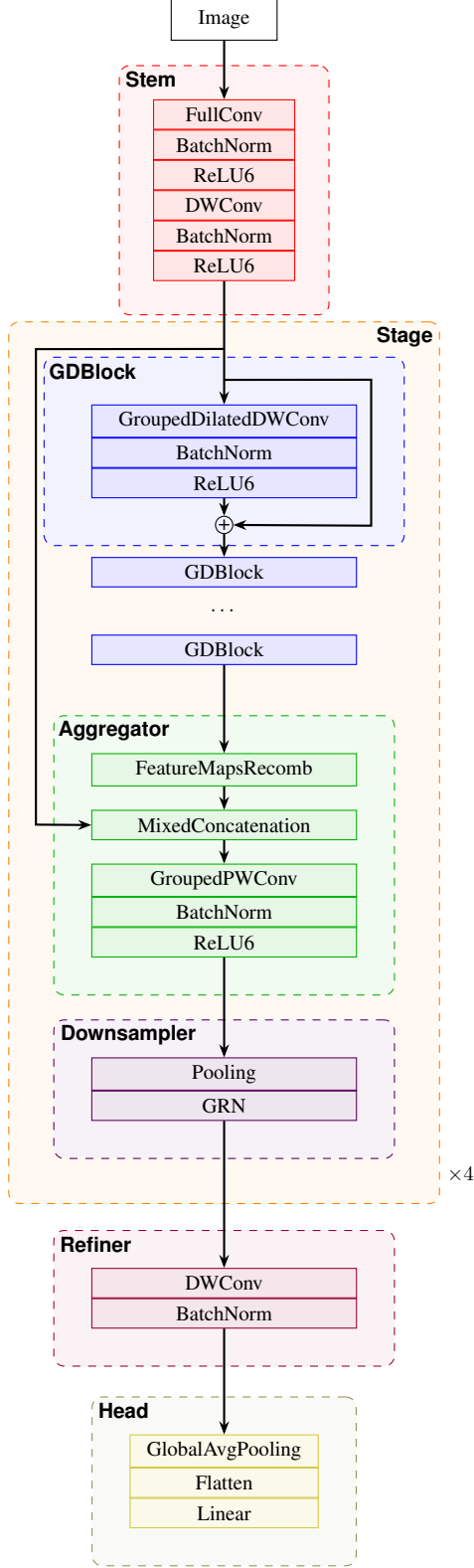


Figure 1. GlimmerNet: the initial *Stem* block reduces spatial dimensions, 4 *Stage* blocks extract representations efficiently, *Refiner* and *Head* align features and perform classification.

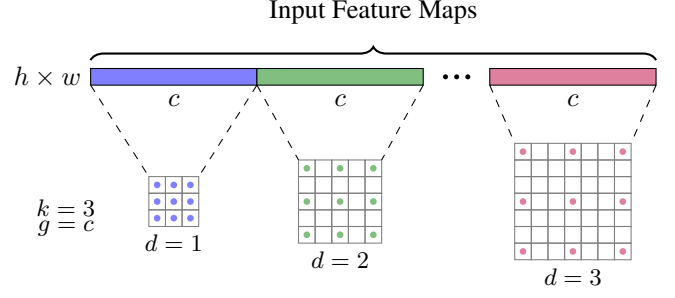


Figure 2. **GroupedDilatedDWConv** - The grouped dilated depthwise convolution:  $k$  - kernel size,  $g$  - group size,  $d$  - dilation level. Each group has  $c$  filters. Input tensor has shape  $(h, w, m \cdot c)$ , where  $m$  is number of groups.

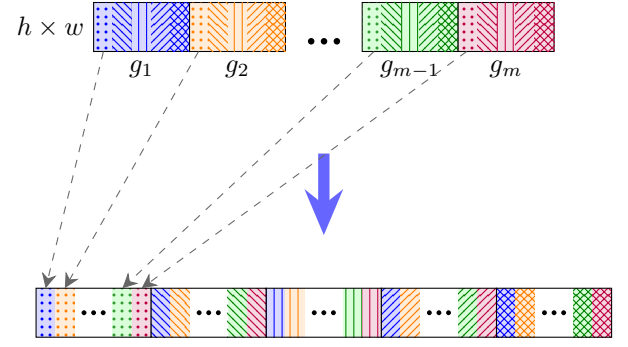


Figure 3. **FeatureMapsRecomb** - Get feature maps from the same index inside each of input  $m$  groups and form new group. Therefore, there will be  $c$  output groups with  $m$  feature maps in each.

TakuNet [20]. This reduction directly contributes to a lower overall parameter count.

### 3.3. GDBlock

*GDBlock* (Grouped Dilations Block) is composed of a grouped dilated depthwise convolution, followed by Batch Normalization [10] and a ReLU6 activation. An identity skip connection is added to the block's output via summation, ensuring gradient flow and improving convergence.

The **grouped dilated depthwise convolution** (*Grouped-DilatedDWConv*), illustrated in Fig. 2, builds on the idea of grouped convolutions, which originated in the AlexNet [12] architecture and were notably popularized by ResNeXt [33]. That design follows a split-transform-merge strategy: the input is split into groups, each group is processed with identical transformations (uniform kernels), and the outputs are merged by summation. The number of such parallel transformations is referred to as *cardinality*, which the authors [33] introduced as a new architectural dimension-alongside depth and width, with a strong influence on model performance. They showed that increasing



cardinality can be a more effective way to boost accuracy than increasing depth or width, without necessarily increasing the number of parameters.

Inspired by this, we apply grouped convolutions to separate subsets of input features. However, to enhance architectural efficiency, we do not use uniform kernels across groups. Instead, each group uses a **different dilation rate**, allowing a single convolutional pass to capture features at multiple receptive field scales. As illustrated in Fig. 2, we dedicate  $c$  feature maps to each of  $m$  groups. Each group is processed with convolutional filter with the same kernel size  $k$ , but distinctive dilation rate  $d$ . Moreover, in contrast to the dense convolutions commonly used in grouped setups, we employ **depthwise convolutions** within each of  $m$  groups, resulting in significant parameter savings. This design is inspired by the MixConv [28] approach, which varies kernel sizes across depthwise convolution groups. However, rather than increasing kernel sizes, which would raise parameter counts, we vary the dilation rate. Dilation changes the spatial sampling pattern without increasing the number of parameters, enabling a broader and more diverse receptive field at no additional computational cost.

The *GDBlocks* applies depthwise convolutions over  $m$  channel groups, each executed with a different dilation rate. Let the input tensor be  $X \in \mathbb{R}^{h \times w \times C}$ , divided into  $m$  groups of size  $c = C/m$ . For the  $i$ -th group, we assign dilation  $d_i$ , enabling each group to extract features with a distinct receptive field without increasing kernel size or FLOPs. Formally, the output feature map of the  $i$ -th group is:

$$Y^i = \text{BN}(\text{ReLU6}(\text{DWConv}(X^i, d_i))), i \in [1, m]. \quad (1)$$

As a result, each group of  $c$  channels within the *Stage* is consistently processed with the same dilation rate across all *GDBlocks*. This design allows each of the  $m$  groups to specialize in capturing features at a specific granularity, determined by its assigned receptive field size.

### 3.4. Aggregator

The *Aggregator* provides an efficient mechanism for inducing cross-channel correlations in the output tensor produced by the chain of *GDBlocks* within a given *Stage*.

The first step involves **feature map recombination across the channel dimension**, as illustrated in Fig. 3. Each group  $g_i$  in the input tensor corresponds to a specific dilation rate from the *GDBlocks*. Formally, the *GDBlocks*' output feature map  $Y_i \in \mathbb{R}^{h \times w}$  is moved to the index  $\ell$  defined as:

$$\ell = \underbrace{((i \bmod c) - 1)m}_{\text{whole output groups offset value}} + \underbrace{\lceil i/c \rceil}_{\text{index in group}}. \quad (2)$$

This indexing shifts each feature map so that responses from different dilation groups are aligned along the channel dimension. Effectively, we reorganize the feature maps so that features at the same index within each  $g_i, i \in [1, m]$ , are grouped together to form a new set of  $c$  groups, each of size  $m$ . As a result, each newly formed group contains features extracted using all  $m$  distinct receptive field sizes, one from each original group. Compared to TakuNet [20] blocks, where depthwise convolutions operate with a single dilation per stage, *GDBlock* captures **multi-scale context within a single convolutional unit**, allowing us to **use fewer blocks per stage while maintaining or improving accuracy**.

Following a design similar to the TakuNet [20] *Stage*, we enhance the aggregated features by incorporating a skip connection from the *Stage*'s original input. The output of the *FeatureMapsRecomb* operation is mixed with the input tensor through channel-wise interleaving in the *MixedConcatenation* block. Both the recombined and input tensors have a channel size of  $m \cdot c$ , resulting in a concatenated tensor of size  $2 \cdot m \cdot c$ .

Effective **aggregation** is then performed by the **grouped pointwise convolution** (*GroupedPWConv*) block. Here, we apply a grouped  $1 \times 1$  convolution with a group size of  $2 \cdot m$ , aligning with the structure of the interleaved groups formed in the previous step. This approach allows each group to aggregate features across multiple receptive field granularities efficiently, while keeping the number of parameters low. Unlike a standard dense  $1 \times 1$  convolution that would require  $2 \cdot m \cdot c$  input channels, this grouped version operates with just  $2 \cdot m$  input channels per group. The convolution is followed by Batch Normalization [10] and ReLU6 activation to stabilize training and introduce non-linearity.

### 3.5. Optimization Strategy of GDBlocks

To ensure the *GDBlock* remains computationally efficient for real-time UAV deployment, we follow a principled optimization strategy balancing receptive field diversity, cross-channel mixing, and FLOP budget.

- **Group cardinality selection ( $m$ )**

Larger  $m$  increases receptive field diversity but reduces cross-channel interaction. Consequently, we selected  $m = 4$  as an optimal compromise for the specific application of emergency response.

- **Dilation schedule  $\{d_1 \dots d_m\}$**

Dilation increases receptive field without adding parameters or FLOPs, enabling multiscale perception at constant cost. We assign increasing dilation across groups  $d = \{1, 2, 2, 3\}$  ensuring each block captures short, medium and long range context in a single pass. Kernel of size 3 with dilation 3 covers spatial range  $7 \times 7$ . Since the final *Stage*'s input is spatially downsampled to  $7 \times 7$ , we limited maximal value for dilation to 3. Ablation in Table 8

confirms that dilated grouping improves F1 from 0.928 to 0.936 even without *Aggregator*.

- **Depth vs. stage width strategy**

Instead of stacking many depthwise layers (as in TakuNet [20]), *GDBlocks* reduce per-stage depth while expanding receptive field coverage, improving accuracy while lowering FLOPs. Table 9 shows reducing depth only minimally impacts accuracy, enabling structural efficiency scaling.

### 3.6. Downsampler

This block serves as a lightweight spatial scaling operator, utilizing pooling operations followed by Global Response Normalization (GRN) [32]. In the first three *Stages*, spatial downsampling is performed using max pooling, while in the final *Stage*, we apply average pooling instead.

### 3.7. Refiner and Classification Head

The final two blocks, *Refiner* [20] and *Head* [20], prepares the output of the *Stages* for the final class probability prediction.

The *Refiner* [20] consists of a simple  $3 \times 3$  depthwise convolution followed by Batch Normalization [10], serving to refine the extracted features. The *Head* [20] block then applies Global Average Pooling, reducing the spatial dimensions to a single value per channel. Finally, the resulting embedding vector is passed through a fully connected layer that maps it to the desired number of output classes.

## 4. Experiments

### 4.1. Architecture and Training

The architectural choices in our network are primarily centered around the configuration of the *GDBlock*. Specifically, the number of *GDBlocks* across the 4 *Stages* is set to [4, 4, 4, 1]. All *GDBlocks* are consistent in their structure, employing grouped dilated depthwise convolutions with 4 groups and dilation rates of [1, 2, 2, 3]. The output channel dimensions across *Stages* are [40, 80, 160, 240]. Downsampling within the *Downsampler* block is performed using pooling operations with a kernel size of 2 and stride of 2.

The training setup is identical to that of TakuNet [20], allowing us to isolate and evaluate the impact of our architectural modifications on performance. Training was conducted over 300 epochs with a batch size of 64, using the RMSProp [29] optimizer configured with a decay of 0.9 and momentum of 0.9. The learning rate at epoch  $i$  is controlled by a step-based scheduler defined as:

$$\eta_i = \eta_0 \cdot \gamma^{\lfloor \frac{i}{step\_size} \rfloor} \quad (3)$$

where  $\eta_0 = 1 \cdot 10^{-3}$  is the initial learning rate,  $\gamma = 0.975$  is the multiplicative factor, and the *step\_size* is period of

Class	Train	Test	Total
Collapsed Building	365	146	511
Fire/Smoke	373	148	521
Flood	376	150	526
Traffic Accidents	346	139	485
Normal	2,850	1,540	4,390
<b>Total Per Set</b>	<b>4,310</b>	<b>2,123</b>	<b>6,433</b>

Table 1. AIDER [13] dataset distribution per class

Class	Train	Validation	Test	Total
Earthquakes	1,927	239	239	2,405
Flood	4,063	505	502	5,070
Fire	3,509	436	436	4,384
Normal	3,900	487	477	4,864
<b>Total</b>	<b>13,399</b>	<b>1,670</b>	<b>1,654</b>	<b>16,723</b>

Table 2. AIDERv2 [23] dataset distribution per class

applying multiplication set to 2 epochs. The only regularization applied during training is weight decay, with a value of  $1 \cdot 10^{-5}$ .

We use the standard cross-entropy loss applied to the softmax probabilities produced by the *Head* block for final classification. For data augmentation, we adopt the same set of transformations used in EmergencyNet [14], the first architecture specifically designed for the expanded AIDER [13] dataset. The applied augmentations are listed in Table 3.

### 4.2. Datasets

The original aerial imagery dataset for emergency situation classification, AIDER [13], consists of hand-collected images captured under various conditions, across different seasons, times of day, and in both natural and urban environments. The dataset includes multi-resolution images categorized into four emergency classes and one non-emergency (Normal) class.

The same authors later expanded this dataset in their follow-up work, EmergencyNet [14]. However, due to copyright restrictions, a significant number of images had to be excluded from the publicly available version. The resulting class distribution is presented in Table 1. Notably, the emergency classes are heavily underrepresented in both the training and testing subsets, especially when compared to the dominant Normal class. Additionally, this dataset does not include a dedicated validation set, which limits its utility for model selection and generalization evaluation.

The AIDERv2 [23] dataset is a large-scale aerial emergency recognition benchmark designed for UAV-based disaster monitoring. It consists of multi-resolution RGB images (typically 256–1024 pixels on the long side) captured from varying flight altitudes and viewing angles, including

Transform	Description
HorizontalFlip	Random horizontal flip with probability 0.5.
IAAPerspective	Perspective distortion simulating viewing the scene from a shifted angle.
GridDistortion	Grid-based geometric warping with elastic-style distortions.
CoarseDropout	Randomly removes rectangular regions (holes), simulating occlusion.
GaussNoise	Adds Gaussian noise with variance sampled from a defined range.
ShiftScaleRotate	Applies random translation, scaling, and small-angle rotation.
ColorJitter	Random changes in brightness, contrast, saturation, and hue.
Blur	Applies random blurring to simulate motion or defocus.
ToGray	Converts image to grayscale with probability $p$ .
RandomGamma	Applies gamma correction with gamma sampled from a given range.

Table 3. Image augmentation transformations used in our experiments.

nadir, oblique, and forward-facing perspectives. Unlike the original AIDER [13] dataset, which offered a limited number of samples per category, AIDERv2 [23] is fully open-access and significantly more diverse in visual conditions and scene composition.

The dataset includes three emergency categories (Earthquake, Fire, Flood) and one non-emergency category (Normal). Images originate from dense urban regions, coastal areas, forests, industrial zones, and rural landscapes, covering a range of weather conditions, seasonal appearances, and daytime lighting variations. This diversity makes classification more challenging due to variations in scale, background clutter, structural damage patterns, smoke coverage, and color shifts in fire and flood scenes.

AIDERv2 provides independent training, validation, and test splits, enabling reliable benchmarking without custom partitioning. The distribution of each class is presented in Table 2. Compared to AIDER [13], the AIDERv2 [23] dataset offers:

- a larger and more balanced category distribution,
  - increased intra-class variation and visual complexity,
  - improved realism for UAV-emergency surveillance evaluation,
  - standardized evaluation splits for fair model comparison.
- These characteristics make AIDERv2 [23] particularly suitable for assessing lightweight CNN architectures intended for onboard UAV inference, where robustness across varied conditions is crucial.

## 4.3. Results

We evaluated the proposed model in two key aspects: classification accuracy and model size, the latter serving as an indicator of computational efficiency. Given the class imbalance in the dataset, the most appropriate performance metric is the weighted F1-score, which is widely adopted in works applied on the AIDER family of datasets, such as DiRecNetV2 [22], EmergencyNet [14], TinyEmergencyNet [19] and TakuNet [20]. Model size is assessed using multiple criteria, including the number of parameters, memory footprint (MB), and FLOPs (floating-point operations).

### 4.3.1. Performance on the AIDERv2 Dataset

A full comparison across metrics is presented in Table 4. We successfully reproduced the results of TakuNet [20] on the AIDERv2 [23] dataset. Results for other concurrent models are taken directly from the same work. The baseline models of TakuNet [20] are sourced directly from TorchVision library, except EmergencyNet [14] and TinyEmergencyNet [19]. They are reimplemented by authors, due to the absence of official code. For a fair comparison, all models are trained in 300 epochs with batch size 64. The input size for all models on AIDERv2 [23] is  $224 \times 224$ . TakuNet [20] authors report results for  $FP = 16$  precision alongside the default  $FP = 32$ , since one of their contribution is  $FP$  optimization without drop in accuracy. The experiments are performed using GeForce RTX 3090 and Intel i9-9900K.

TakuNet [20] is a recent architecture that demonstrated a significant reduction in computational cost while maintaining near state-of-the-art accuracy. Our proposed model, **GlimmerNet**, further improves on this by achieving a **16.66% reduction in parameters** and **29% fewer FLOPs**, while also delivering the **highest F1-score of 0.966**.

To quantify the contribution of data augmentations, we trained a baseline model without any augmentation, which achieved an F1-score of 0.945.

In addition to the overall evaluation, we conducted a per-class performance analysis to better understand model behavior across different event types (Table 7). The results reveal that the Earthquakes class consistently shows weaker performance across all metrics compared to Flood, Fire, and Normal images. This indicates that earthquake-related patterns are more challenging for the model to learn, likely due to higher intra-class variability or less distinctive visual cues. Consequently, future work should focus on a deeper examination of the Earthquakes class, its visual characteristics, data diversity, and potential ambiguities.

### 4.3.2. Performance on the AIDER Dataset

To ensure a fair comparison with previous UAV-oriented methods, we also evaluate GlimmerNet on the original AIDER [13] dataset. Results are presented in Table 5. Training setup is identical to the main experiment. Num-

Model	Parameters ↓	Model Size (MB) ↓	F1-score ↑	FLOPs ↓
ConvNext Tiny [15]	27,820,000	111.29	0.940	4.46G
GCVit XXtiny [4]	11,480,000	45.93	0.932	1.94G
Vit Tiny [1]	5,530,000	22.1	0.873	1.08G
Convit Tiny [2]	5,520,000	22.07	0.871	1.08G
MobileViT s [17]	4,940,000	19.76	0.855	1.42G
MobileViT V2 0100 [18]	4,390,000	17.56	0.875	1.41G
EfficientNet-B0 [27]	4,010,000	16.05	0.862	0.41G
MnasNet [26]	3,110,000	12.43	0.897	0.34G
MobileNetV2 [21]	2,230,000	8.92	0.893	0.33G
MobileViT xs [17]	1,930,000	7.74	0.837	0.71G
ShuffleNet V2 [16]	1,260,000	5.03	0.852	0.15G
MobileViT V2 050 [18]	1,110,000	4.46	0.834	0.36G
MobileViT xxs [17]	950,000	3.81	0.859	0.26G
MobileNetV3 Small [6]	930,000	3.72	0.868	0.06G
DiRecNetV2 [22]	799,380	3.20	0.964	1.09G
SqueezeNet [9]	730,000	2.90	0.845	0.26G
EmergencyNet [14]	90,704	0.36	0.952	61.96M
TinyEmergencyNet [19]	39,075	0.16	0.928	31.57M
TakuNet <sub>FP=16</sub> [20]	37,444	0.15	0.958	31.38M
TakuNet <sub>FP=32</sub> [20]	37,444	0.15	0.954	31.38M
GlimmerNet (ours)	<b>31,204</b>	<b>0.12</b>	<b>0.966</b>	<b>22.26M</b>

Table 4. Comparison of model number of parameters, memory size, F1-score and FLOPS on AIDERv2 [23] test set.

Model	Parameters ↓	Model Size (MB) ↓	F1-score ↑	FLOPs ↓
VGG16 [24]	14,840,133	59.36	0.601	17.62G
ResNet50 [5]	23,518,277	94.07	0.917	4.83G
SqueezeNet [9]	737,989	2.95	0.890	845.38M
EfficientNet-B0 [27]	4,013,953	16.06	<b>0.950</b>	479.68M
MobileNetV2 [21]	2,230,277	8.92	0.930	371.82M
MobileNetV3 [6]	4,208,437	16.83	0.915	265.02M
ShuffleNet [16]	1,258,729	5.03	0.908	176.82M
EmergencyNet [14]	90,963	0.360	0.936	77.34M
TinyEmergencyNet [19]	39,334	0.160	0.895	36.30M
TakuNet <sub>FP=16</sub> [20]	37,685	0.15	0.943	35.93M
TakuNet <sub>FP=32</sub> [20]	37,685	0.15	0.938	31.38M
GlimmerNet (ours)	<b>29,525</b>	<b>0.12</b>	0.942	<b>25.45M</b>

Table 5. Comparison of model number of parameters, memory size, F1-score and FLOPS on AIDER [13] test set.

ber of blocks per stage is [4, 4, 3, 1] and input resolution is  $240 \times 240$ .

The network achieves an F1-score of 0.942, near by the best reported performance of TakuNet [20] while requiring only 29.5K parameters and 29% fewer FLOPs. This confirms that GlimmerNet’s efficiency gains are not limited to the improved AIDERv2 [23] dataset, but extend to earlier benchmarks as well.

#### 4.4. Generalization Ability On Generic Visual Tasks

To further evaluate the robustness and generalization capacity of the proposed architecture beyond UAV-specific emer-

gency monitoring, we extended our analysis to a general-purpose image classification benchmark. This experiment aims to verify that GlimmerNet is not specialized solely for domain-specific feature distributions but can also learn effectively from diverse visual concepts.

We selected the TinyImageNet [25] dataset, a reduced version of ImageNet comprising 200 object categories, each with 500 training and 50 validation samples at a spatial resolution of  $64 \times 64$  pixels. TinyImageNet [25] provides a demanding benchmark for compact models due to its high inter-class variability, limited sample size per class, and smaller image resolution. While the full ImageNet dataset



Model	Params(M)↓	FLOPs(M)↓	Accuracy(%)↑	Notes
ResNet-18 [5]	11.7	1800	65–70	Verified across re-implementations
MobileNetV2 [21]	2.2	330	58–62	Common open-source benchmarks
ShuffleNet V2 (0.5x) [16]	1.26	150	55–60	Public leaderboard reports
TinyNet-A [3]	6.2	339	59–63	timm community runs
MixNet-S [28]	4.1	256	60–63	timm community runs
WaveMix-Lite/WaveMix-32 [11]	1–2	250	64–67	Reported in WaveMix paper
GlimmerNet (ours)	0.24	28	47.08	Scaled-up configuration

Table 6. Comparison of model number of parameters, FLOPS and Accuracy on TinyImageNet [25] dataset. Baseline results are reported from publicly available TinyImageNet [25] re-implementations in the timm [31] repository and open community benchmarks, since the original papers do not provide TinyImageNet [25] results.

Class	Precision	Recall	F1-score	AUC
Earthquakes	0.928	0.921	0.924	0.995
Flood	0.991	0.975	0.983	0.999
Fire	0.966	0.972	0.969	0.998
Normal	0.963	0.975	0.969	0.998

Table 7. Per-class performance metrics on the AIDERv2 [23] test set.

would offer a more comprehensive evaluation, experiments at that scale were beyond our computational budget (single RTX 3090 GPU). Hence, TinyImageNet [25] serves as a practical proxy to assess GlimmerNet’s ability to generalize to large-scale visual domains.

For this experiment, GlimmerNet was scaled up from its original UAV-focused design to increase representational capacity while maintaining lightweight efficiency. The number of stages was expanded from 4 to 6, with the number of grouped dilated blocks (*GDBlocks*) per stage defined as [6, 5, 5, 4, 3, 1]. The corresponding stage output channel dimensions were set to [40, 80, 160, 320, 640, 640]. Each *GDBlock* employed grouped dilated depthwise convolutions with 5 groups and dilation rates [1, 1, 2, 2, 3], followed by grouped pointwise aggregation for cross-group fusion.

Training was performed using the AdamW optimizer with a learning rate of  $\eta_0 = 2 \cdot 10^{-3}$ , decayed by a cosine annealing scheduler over 300 epochs with batch size of 128. Label smoothing, random resized cropping, horizontal flipping, and dropout were used to enhance regularization and prevent overfitting.

These results confirm that GlimmerNet generalizes effectively beyond UAV-based imagery, preserving competitive performance on a dataset with 200 heterogeneous object classes despite its extremely small computational footprint. This indicates that the grouped-dilated feature extraction mechanism is transferable across domains and scales, supporting GlimmerNet’s suitability as a compact, general-purpose backbone for edge-deployed vision applications.

Configuration	FLOPs	F1-score
Baseline - DW Conv2D (TakuNet)	4.75M	0.928
GDDWConv	4.41M	0.933
GDDWConv + Aggs	4.41M	0.936

Table 8. Ablation study on Grouped Dilated Depthwise Convolutions and Aggregators. The model size is kept nearly constant, while employing GlimmerNet’s building blocks produces a noticeable gain in accuracy.

## 4.5. Ablation Studies

### 4.5.1. Ablation on GroupedDilatedDWConvs and Aggregators

To quantify the contribution of the proposed modules, we conducted an ablation study on a reduced-complexity variant of GlimmerNet containing approximately 4.7M FLOPs, trained with the same optimization and augmentation setup as in the main AIDERv2 [23] experiment. In this version, the grouped dilated depthwise convolutions (*GroupedDilatedDWConv*) and *Aggregator* modules were sequentially enabled to isolate their effects.

As a baseline, all *GroupedDilatedDWConvs* and *Aggregators* were replaced by standard depthwise Conv2D operators similar to those employed in TakuNet. The configuration of [1, 1, 1, 1] blocks and widths [8, 16, 24, 120] achieved an F1-score of 0.928 on the AIDERv2 [23] test set. Replacing these depthwise convolutions with *GroupedDilatedDWConvs* of channel widths [8, 16, 24, 160] and dilation patterns [[1, 1, 2, 3], [1, 1, 2, 3], [1, 2, 2, 3], [1, 2, 2, 3]] increased the test F1-score to 0.933, indicating that the multi-scale receptive-field grouping improves discriminative representation. When the *Aggregator* modules were additionally inserted for cross-group channel recombination, the performance further improved to 0.936, confirming that the *Aggregator* complements the *GroupedDilatedDWConv* features by enhancing cross-scale information exchange. The results in Table 8 demonstrate that both modules independently contribute to accuracy improvements while maintaining the same computational budget.

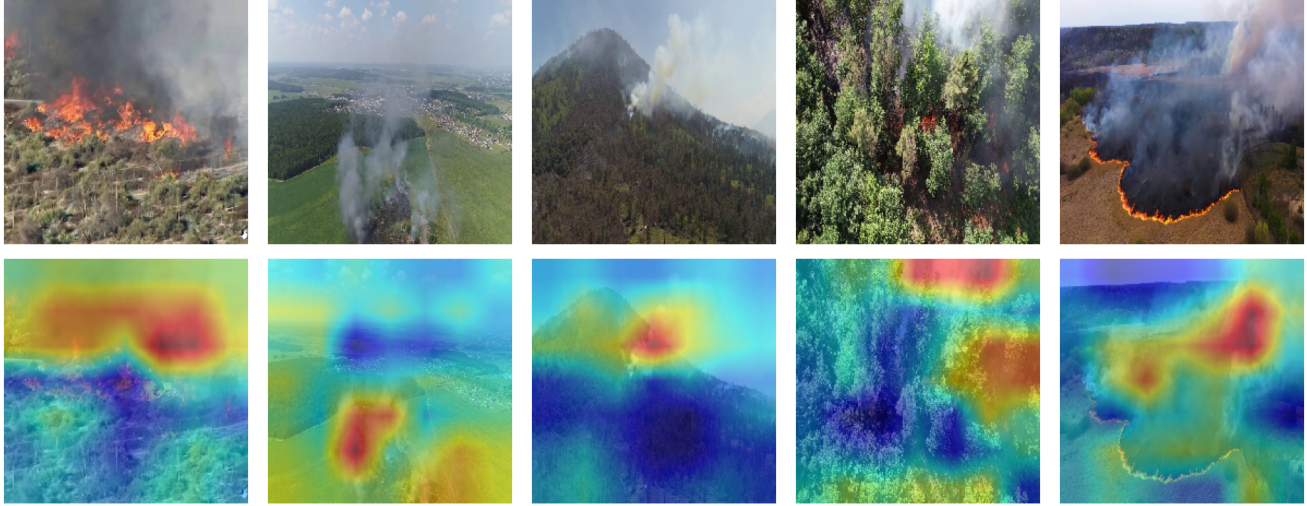


Figure 4. Class activation maps of the last *Stage*’s *Aggregator* for image samples of the Fire class. Blue represents the lowest and red is for the highest values.

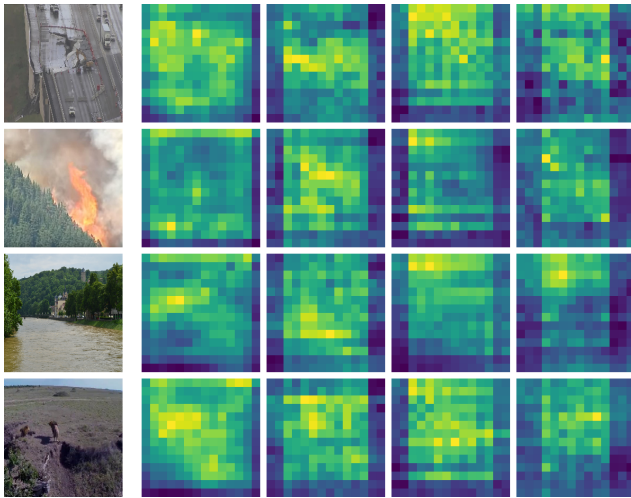


Figure 5. Feature maps per group of the last *GroupedDilatedDW-Conv* block in *Stage* 3, averaged along channels. Respective inputs for Earthquake, Fire, Flood and Normal class are on the left side.

#### 4.5.2. Number of GDBlocks

A key contribution of this work is the reduction in model size, achieved through the proposed *GDBlock* design. To better understand its impact, we conducted an ablation study analyzing the effect of the number of *GDBlocks* per *Stage* on classification accuracy. The evaluation was carried out on the validation split of the dataset. Detailed results are presented in Table 9. As expected, reducing the number of *GDBlocks* per *Stage* decreases the network’s capacity, leading to a drop in F1-score.

GDBlocks	Parameters	FLOPs	F1-score
(4, 4, 4, 1)	<b>31,204</b>	<b>22.26M</b>	<b>0.956</b>
(4, 3, 2, 1)	26,404	22.01M	0.954
(4, 2, 2, 1)	25,444	21.89M	0.949
(1, 1, 1, 1)	21,124	20.92M	0.944

Table 9. Reduction of number of *GDBlocks* per *Stage*. F1-score is calculated on the validation dataset.

#### 4.6. Qualitative Analysis

Fig.4 presents selected representative samples from the Fire class, overlaid with Class Activation Maps (CAMs). These activations are the outputs of the *Aggregator* block in the final *Stage* of the network. The defining visual attributes of this class, fire and smoke, appear in varying proportions, relative positions, and distances within each image. GlimmerNet consistently activates in regions containing smoke and fire. In the left three examples, these regions are spatially connected. Notably, even when fire and smoke are spatially separated, as seen in the right two examples, GlimmerNet still activates in both regions. This suggests that the model captures a more global representation too, rather than relying solely on localized features.

In another study, we perform a qualitative analysis of the feature representations learned across different groups in the *GroupedDilatedDWConv* layer. We focus on the output of the last *GDBlock* in *Stage* 3, selected for its intermediate spatial resolution ( $14 \times 14$ ), well-suited for visualization while still maintaining sufficient detail for interpretability. In Fig. 5, we present feature maps for each of the four groups (columns in the feature map matrix), averaged

across the channel dimension. Each row corresponds to one input image shown on the left. One of the most notable observations is that each group captures distinct activation patterns, indicating a lack of redundancy between them. This suggests that the groups specialize in extracting complementary information, validating our architectural choice of assigning different dilation rates to each group to encourage diverse receptive field learning. Even if two groups have the same dilation rate, like two central groups in our case, their feature maps are distinctive.

## 5. Conclusion

This work contributes to the emerging research area of applying deep learning models for emergency event recognition from aerial imagery captured by UAVs. Unlike conventional approaches that rely on offline processing, our goal is to enable on-device inference under the constraints of embedded-level hardware commonly used in UAV systems.

We propose a novel architecture, GlimmerNet, that integrates Grouped Dilated Convolutional Blocks with an innovative feature map recombination strategy prior to point-wise aggregation. This mechanism enhances cross-channel representation alignment and contributes significantly to the model’s efficiency. Our design achieves substantial reductions in model size, notably 16.66% fewer parameters and 29% fewer FLOPs compared to recent state-of-the-art architectures, while still attaining the highest F1-score (0.966) among evaluated models on the AIDERv2 [23] dataset.

### 5.1. Future Work

While GlimmerNet demonstrates strong performance for single-sensor RGB aerial imagery, several extensions are anticipated to further improve robustness and deployment readiness in real-world UAV missions. A natural next direction is to extend the architecture toward multi-sensor fusion, incorporating thermal, NIR, or SAR modalities alongside RGB. The *GroupedDilatedDWConv* formulation is inherently compatible with modality-partitioned feature extraction, where each sensor can be assigned its own grouped dilation pathway and later merged using a cross-modal *Aggregator*. This enables scene understanding even under degraded visibility (nighttime, smoke, fog), where RGB input alone is insufficient.

A second direction focuses on hardware-efficient deployment. Future work includes quantization-aware training, structured pruning of redundant dilation groups, and mixed-precision execution optimized for Jetson-class UAV boards. Benchmarking inference on embedded platforms will allow us to evaluate energy consumption and operational endurance, critical factors for real-time aerial monitoring.

A current limitation is that deep learning frameworks do not natively support **heterogeneous dilation configurations**

**inside grouped depthwise convolutions**. As a result, the proposed *GroupedDilatedDWConv* block is implemented in Python/PyTorch rather than as a low-level CUDA/C++ kernel. The absence of a highly optimized backend restricts real-time inference evaluation, and therefore latency benchmarking and kernel-level optimization remain a key focus of future work. Efficient implementation will allow FPS-level UAV testing, enabling fair runtime comparisons against other lightweight architectures.

## References

- [1] Alexey Dosovitskiy. An image is worth 16x16 words: Transformers for image recognition at scale. *arXiv preprint arXiv:2010.11929*, 2020. 2, 3, 8
- [2] Stéphane d’Ascoli, Hugo Touvron, Matthew L Leavitt, Ari S Morcos, Giulio Biroli, and Levent Sagun. Convit: improving vision transformers with soft convolutional inductive biases\*. *Journal of Statistical Mechanics: Theory and Experiment*, 2022(11):114005, Nov. 2022. 8
- [3] Kai Han, Yunhe Wang, Qiulin Zhang, Wei Zhang, Chunjing Xu, and Tong Zhang. Model rubik’s cube: Twisting resolution, depth and width for tinynets. *ArXiv*, abs/2010.14819, 2020. 9
- [4] Ali Hatamizadeh, Hongxu Yin, Greg Heinrich, Jan Kautz, and Pavlo Molchanov. Global context vision transformers. In *International Conference on Machine Learning*, pages 12633–12646. PMLR, 2023. 8
- [5] Kaiming He, X. Zhang, Shaoqing Ren, and Jian Sun. Deep residual learning for image recognition. *2016 IEEE Conference on Computer Vision and Pattern Recognition (CVPR)*, pages 770–778, 2015. 8, 9
- [6] Andrew Howard, Mark Sandler, Grace Chu, Liang-Chieh Chen, Bo Chen, Mingxing Tan, Weijun Wang, Yukun Zhu, Ruoming Pang, Vijay Vasudevan, et al. Searching for mobilenetv3. In *Proceedings of the IEEE/CVF international conference on computer vision*, pages 1314–1324, 2019. 3, 8
- [7] Andrew G Howard. Mobilenets: Efficient convolutional neural networks for mobile vision applications. *arXiv preprint arXiv:1704.04861*, 2017. 1, 2
- [8] Andrew G. Howard, Mark Sandler, Grace Chu, Liang-Chieh Chen, Bo Chen, Mingxing Tan, Weijun Wang, Yukun Zhu, Ruoming Pang, Vijay Vasudevan, Quoc V. Le, and Hartwig Adam. Searching for mobilenetv3. *2019 IEEE/CVF International Conference on Computer Vision (ICCV)*, pages 1314–1324, 2019. 2
- [9] Forrest N Iandola. Squeezenet: Alexnet-level accuracy with 50x fewer parameters and < 0.5 mb model size. *arXiv preprint arXiv:1602.07360*, 2016. 2, 8
- [10] Sergey Ioffe and Christian Szegedy. Batch normalization: Accelerating deep network training by reducing internal covariate shift. *ArXiv*, abs/1502.03167, 2015. 3, 4, 5, 6
- [11] Pranav Jeevan, Kavitha Viswanathan, Anandu A S, and Amit Sethi. Wavemix: A resource-efficient neural network for image analysis, 2024. 3, 9
- [12] Alex Krizhevsky, Ilya Sutskever, and Geoffrey E Hinton. Imagenet classification with deep convolutional neural networks. In F. Pereira, C.J. Burges, L. Bottou, and K.Q. Wein-



- berger, editors, *Advances in Neural Information Processing Systems*, volume 25. Curran Associates, Inc., 2012. 4
- [13] Christos Kyrkou and Theodoris Theodoridis. Deep-learning-based aerial image classification for emergency response applications using unmanned aerial vehicles. In *CVPR workshops*, pages 517–525, 2019. 6, 7, 8
- [14] Christos Kyrkou and Theodoris Theodoridis. Emergencynet: Efficient aerial image classification for drone-based emergency monitoring using atrous convolutional feature fusion. *IEEE Journal of Selected Topics in Applied Earth Observations and Remote Sensing*, 13:1687–1699, 2020. 2, 3, 6, 7, 8
- [15] Zhuang Liu, Hanzi Mao, Chao-Yuan Wu, Christoph Feichtenhofer, Trevor Darrell, and Saining Xie. A convnet for the 2020s. In *Proceedings of the IEEE/CVF conference on computer vision and pattern recognition*, pages 11976–11986, 2022. 2, 8
- [16] Ningning Ma, Xiangyu Zhang, Hai-Tao Zheng, and Jian Sun. Shufflenet v2: Practical guidelines for efficient cnn architecture design. In *Proceedings of the European conference on computer vision (ECCV)*, pages 116–131, 2018. 2, 3, 8, 9
- [17] Sachin Mehta and Mohammad Rastegari. Mobilevit: lightweight, general-purpose, and mobile-friendly vision transformer. *arXiv preprint arXiv:2110.02178*, 2021. 2, 8
- [18] Sachin Mehta and Mohammad Rastegari. Separable self-attention for mobile vision transformers. *arXiv preprint arXiv:2206.02680*, 2022. 2, 8
- [19] Obed Mogaka, Rami Zewail, Koji Inoue, and Mohammed Sayed. Tinyemergencynet: a hardware-friendly ultra-lightweight deep learning model for aerial scene image classification. *Journal of Real-Time Image Processing*, 21:51, 03 2024. 2, 3, 7, 8
- [20] Daniel Rossi, Guido Borghi, and Roberto Vezzani. Takunet: An energy-efficient cnn for real-time inference on embedded uav systems in emergency response scenarios. *2025 IEEE/CVF Winter Conference on Applications of Computer Vision Workshops (WACVW)*, pages 339–348, 2025. 1, 2, 3, 4, 5, 6, 7, 8
- [21] Mark Sandler, Andrew Howard, Menglong Zhu, Andrey Zhmoginov, and Liang-Chieh Chen. Mobilenetv2: Inverted residuals and linear bottlenecks. In *Proceedings of the IEEE conference on computer vision and pattern recognition*, pages 4510–4520, 2018. 2, 3, 8, 9
- [22] Demetris Shianios, Panayiotis S. Kolios, and Christos Kyrkou. Direcnetv2: A transformer-enhanced network for aerial disaster recognition. *SN Computer Science*, 5(6), Aug. 2024. 3, 7, 8
- [23] Demetris Shianios, Christos Kyrkou, and Panayiotis S Kolios. A benchmark and investigation of deep-learning-based techniques for detecting natural disasters in aerial images. In *International Conference on Computer Analysis of Images and Patterns*, pages 244–254. Springer, 2023. 1, 2, 3, 6, 7, 8, 9, 11
- [24] Karen Simonyan and Andrew Zisserman. Very deep convolutional networks for large-scale image recognition. *CoRR*, abs/1409.1556, 2014. 8
- [25] Stanford University. Tiny imagenet visual recognition challenge. <https://tinyimagenet.cs231n.stanford.edu/>, 2015. Accessed: October 2025. 8, 9
- [26] Mingxing Tan, Bo Chen, Ruoming Pang, Vijay Vasudevan, Mark Sandler, Andrew Howard, and Quoc V Le. Mnasnet: Platform-aware neural architecture search for mobile. In *Proceedings of the IEEE/CVF conference on computer vision and pattern recognition*, pages 2820–2828, 2019. 8
- [27] Mingxing Tan and Quoc Le. Efficientnet: Rethinking model scaling for convolutional neural networks. In *International conference on machine learning*, pages 6105–6114. PMLR, 2019. 2, 3, 8
- [28] Mingxing Tan and Quoc V. Le. Mixconv: Mixed depthwise convolutional kernels. In *British Machine Vision Conference*, 2019. 1, 3, 5, 9
- [29] Tijmen Tieleman and Geoffrey Hinton. Rmsprop: Divide the gradient by a running average of its recent magnitude. coursera: Neural networks for machine learning. *COURSERA Neural Networks Mach. Learn.*, 17, 2012. 6
- [30] Ashish Vaswani, Noam M. Shazeer, Niki Parmar, Jakob Uszkoreit, Llion Jones, Aidan N. Gomez, Lukasz Kaiser, and Illia Polosukhin. Attention is all you need. In *Neural Information Processing Systems*, 2017. 1
- [31] Ross Wightman. Pytorch image models. <https://github.com/huggingface/pytorch-image-models>, 2019. 9
- [32] Sanghyun Woo, Shoubhik Debnath, Ronghang Hu, Xinlei Chen, Zhuang Liu, In So Kweon, and Saining Xie. Convnext v2: Co-designing and scaling convnets with masked autoencoders. In *Proceedings of the IEEE/CVF Conference on Computer Vision and Pattern Recognition*, pages 16133–16142, 2023. 6
- [33] Saining Xie, Ross B. Girshick, Piotr Dollár, Zhuowen Tu, and Kaiming He. Aggregated residual transformations for deep neural networks. *2017 IEEE Conference on Computer Vision and Pattern Recognition (CVPR)*, pages 5987–5995, 2016. 4
- [34] Xiangyu Zhang, Xinyu Zhou, Mengxiao Lin, and Jian Sun. Shufflenet: An extremely efficient convolutional neural network for mobile devices. *2018 IEEE/CVF Conference on Computer Vision and Pattern Recognition*, pages 6848–6856, 2017. 2